

Erosion rates on different timescales derived from cosmogenic ^{10}Be and river loads: implications for landscape evolution in the Rhenish Massif, Germany

H. Meyer · R. Hetzel · H. Strauss

Received: 2 April 2008 / Accepted: 26 October 2008 / Published online: 14 November 2008
© Springer-Verlag 2008

Abstract We determined erosion rates on timescales of 10^1 – 10^4 years for two catchments in the northeastern Rhenish Massif, in order to unravel the Quaternary landscape evolution in a Variscan mountain range typical of central Europe. Spatially averaged erosion rates derived from in situ produced ^{10}Be concentrations in stream sediment of the Aabach and Möhne watersheds range from 47 ± 6 to 65 ± 14 mm/ka and integrate over the last 9–13 ka. These erosion rates are similar to local rates of river incision and rock uplift in the Quaternary and to average denudation rates since the Mesozoic derived from fission track data. This suggests that rock uplift is balanced by denudation, i.e., the landscape is in a steady state. Short-term erosion rates were derived from suspended and dissolved river loads subsequent to (1) correcting for atmospheric and anthropogenic inputs, (2) establishing calibration curves that relate the amount of suspended load to discharge, and (3) estimating the amount of bedload. The resulting solid mass fluxes (suspended and bedload) agree with those derived from the sediment volume trapped in three reservoirs. However, resulting geogenic short-term erosion rates range from 9 to 25 mm/ka and are only about one-third of the rates derived from ^{10}Be . Model simulations in combination with published sediment yield data suggest that this discrepancy is caused by at least three factors: (1) phases with higher precipitation and/or lower evapotranspiration, (2) rare flood events not captured in the short-term records, and (3) prolonged periods of climatic deterioration

with increased erosion and sediment transport on hillslopes.

Keywords Cosmogenic nuclides · Erosion · Landscape evolution · Central Europe · River loads

Introduction

One of the main factors controlling the topographic evolution of mountain belts is the rate at which material is eroded and removed at the Earth's surface. In tectonically active regions, erosion and rock uplift are acting as two competing processes, and it has been suggested that orogenic systems will tend toward a steady state in which rock uplift is balanced by erosion (Hack 1976; Willet and Brandon 2002). On what timescales such an equilibrium between erosion and uplift is reached and for how long such a steady state can be maintained is a matter of debate. An important prerequisite for resolving these questions is the determination of accurate erosion rates over long timescales. Until recently, however, estimates of erosion rates have mainly relied on measurements of dissolved and suspended load in streams, which typically integrate over periods of a few years to decades (e.g., Milliman and Syvitski 1992; Summerfield and Hulton 1994). For several reasons such sediment gauging methods yield erosion rates that may not be representative for natural erosion over millennial timescales. First, the amount of dissolved load does not only reflect the chemical weathering of rocks in a given catchment, but also comprises atmospheric and anthropogenic inputs. Second, the amount of suspended load depends strongly on stream discharge, but quantification of this relation is notoriously difficult (e.g., Lenzi and Marchi 2000). Third, recent changes in land use and

H. Meyer (✉) · R. Hetzel · H. Strauss
Geologisch-Paläontologisches Institut,
Westfälische Wilhelms-Universität Münster,
Corrensstr. 24, 48149 Münster, Germany
e-mail: hmeye_02@uni-muenster.de

agricultural practices may have accelerated soil erosion (e.g., Pimentel et al. 1995), thereby masking the natural erosion rate. Fourth, most of the sediment may leave a given catchment during infrequent flood events, which may not be captured in sediment gauging studies (e.g., Kirchner et al. 2001; Schaller et al. 2001).

One possibility to obtain natural erosion rates on timescales of 10^3 – 10^5 years is to determine the volume of sediment stored in lakes or valleys (e.g., Zolitschka 1998; Hinderer 2001). Respective quantifications, however, reflect exclusively physical (mechanical) erosion. Contributions from chemical weathering appear as dissolved river loads; hence, will not be captured by sediment storage gauging (Hinderer 2001). In contrast, cosmogenic nuclides allow the quantification of natural background erosion rates in a quasi-holistic approach, considering the entire landscape evolution independent of the weathering type and on timescales of 10^3 – 10^5 years. A short introduction to cosmogenic nuclides is given below, further details can be found in Brown et al. (1995a), Bierman and Steig (1996), Granger et al. (1996), von Blanckenburg (2006), and Granger and Riebe (2007).

Cosmogenic nuclides are continuously produced in the uppermost layer of the Earth's surface by the interaction of cosmic rays with matter (e.g., Lal 1991). Underground, the production rate of cosmogenic nuclides decreases rapidly with depth and therefore, a steadily eroding bedrock surface has a nuclide concentration that is inversely proportional to the rate of erosion (Lal 1991). Likewise, the cosmogenic nuclide concentration in alluvial stream sediment provides a spatially averaged erosion rate for river catchments, if nuclide production in the catchment is equal to nuclide removal by erosion and transport out of the catchment via streams (Brown et al. 1995a; von Blanckenburg 2006). Most widely applied in erosion rate studies is the nuclide ^{10}Be , which is for instance produced in the mineral quartz, but cosmogenic nuclides such as ^{21}Ne and ^{26}Al have also been applied in erosion rate studies (e.g., Kober et al. 2007). Determination of spatially averaged erosion rates with ^{10}Be requires (1) that quartz is distributed uniformly in the catchment, (2) that fluvial sediment is well mixed and its ^{10}Be concentration is representative for the erosion rate of the hillslopes, and (3) that production of ^{10}Be occurs predominantly on the hillslopes, whereas production and decay of ^{10}Be during sediment transport are negligible (e.g., Granger et al. 1996). Whether a catchment exposes only bedrock or is covered by a regolith layer, in which bioturbation or other processes lead to vertical mixing of material, is irrelevant for the application of the method. This is because mixing of an eroding regolith leads to a spatially averaged nuclide concentration in the regolith that is the same as the nuclide concentration of a bedrock surface eroding at the same rate (Granger et al. 1996; Brown et al.

2003). Erosion rates determined with cosmogenic nuclides integrate over a timescale required to erode about ~ 60 cm of bedrock, commonly periods of 10^3 – 10^5 years depending on the erosion rate. Finally, it is important to note that these erosion rates comprise the sum of physical erosion and chemical weathering (e.g., Riebe et al. 2001).

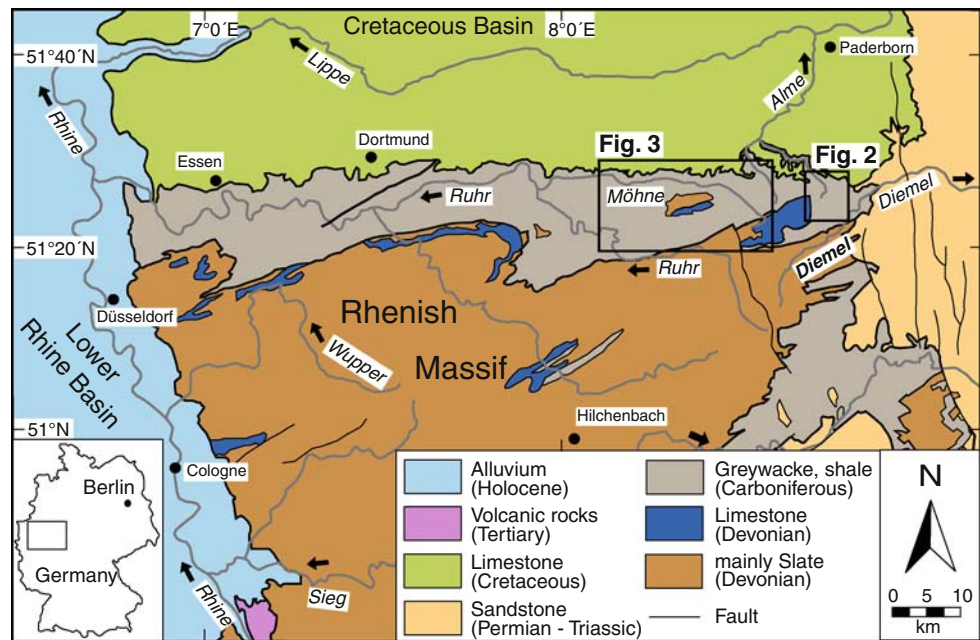
In this study, we derived erosion rates for two catchments in the northeastern Rhenish Massif using cosmogenic ^{10}Be abundances, the chemical composition of river load and the volume of sediment trapped in two reservoirs at the outlets of these catchments. Corrections have been applied for dissolved loads resulting from atmospheric and anthropogenic inputs, and time-integrated suspended loads were quantified. The results obtained by the different methods are compared with each other and their implications for the Late Quaternary landscape development are discussed.

Geological setting and description of the target catchments

The Rhenish Massif is part of the Variscan mountain belt in Central Europe (e.g., Franke 2000), and consists mainly of very low grade to unmetamorphosed Devonian and Carboniferous sediments. It represents one of the best documented cases of Cenozoic plateau uplift in Central Europe (Fuchs et al. 1983). Since the Early Tertiary, the Rhenish Massif experienced a prolonged period of slow rock uplift locally accompanied by volcanic activity (Fuchs et al. 1983). The uplift of the massif has been interpreted as an isostatic response to the heating of the lithosphere by a mantle plume located beneath the Eifel region (e.g., Garcia-Castellanos et al. 2000; Ritter et al. 2001). Detailed investigations of river terraces along the antecedent river Rhine and its tributaries have revealed that rates of river incision and rock uplift are spatially variable and differ in fault-bounded crustal blocks (e.g., Meyer and Stets 1998; Van Balen et al. 2000). In general, the highest uplift rates occur in the western Rhenish Massif, where the elevation of the main terrace level of the Rhine indicates an uplift rate of about 250 mm/ka during the last ~ 800 ka (Meyer and Stets 1998). Outward from this uplift center, the uplift rates generally decrease to less than 50 mm/ka (Van Balen et al. 2000).

We selected two watersheds, the Aabach and the Möhne catchments, in the northeastern part of the Rhenish Massif for the determination of erosion rates on different timescales (Fig. 1). Continued rock uplift in this region during the Quaternary is evident from five terrace levels that stretch along the river Diemel (Fig. 1), although the exact age of the terraces is unknown (Wortmann 1937; Meiburg 1979). The highest terrace occurs up to 135 m above the

Fig. 1 Geological map of the northeastern Rhenish Massif and the adjacent Cretaceous Basin in the north and the Lower Rhine Basin in the east. The locations of the Aabach and Möhne catchments shown in Figs. 2 and 3, respectively, are indicated by black rectangles



present river between the villages Marsberg and Westheim. Assuming that the five terraces formed in the last 1.5–2 Ma as a response to Quaternary climate fluctuations and that river incision reflects rock uplift, they indicate rates of river incision and rock uplift of about 65–90 mm/ka. Both target catchments have not been glaciated and their soil-covered hillslopes dip gently at 3–6°.

The small Aabach catchment (24 km²) has a relief of 150 m and is predominantly underlain by a thick, homogeneous sequence of intercalated greywackes and shales (Fig. 2). It consists of two subcatchments drained by the streams *Große Aa* and *Kleine Aa*. The Möhne catchment has a relief of 450 m and contains the two main subcatchments Möhne (379 km²) and Heve (85 km²). Apart from Late Carboniferous greywackes and shales, the Brilon and Warstein anticlines expose Devonian limestones, slates, and sandstones (Fig. 3). In addition, a narrow belt of Cretaceous sediments along the northern margin of the catchment contains limestone, sandstone, and marl. Discharge in the two target catchments is monitored continuously at six gauging stations operated by three water agencies: *Ruhrverband*, *Aabach-Talsperre*, and *Staatliches Umweltamt Lippstadt* (Table 1). Four of these gauges are located in the Möhne catchment and two are situated in the Aabach watershed (Figs. 2, 3). Land use pattern for both catchments have been extracted from the Corine Land Cover map 2000 of the European Environment Agency (EEA[®], Copenhagen EEA 2000; <http://www.eea.eu.int>) at a resolution of 100 m, listing 44 different categories of land use. We simplified these categories into forest, pasture, farmland, and urban areas (Table 1). In the Aabach catchment and the Heve subcatchment forest prevails, whereas the three other

subcatchments of the Möhne catchment have higher proportions of farmland and urban areas.

Long-term erosion rates determined with ¹⁰Be

Sample collection and preparation

Samples of bedload material (4–6 kg) for ¹⁰Be analysis were either collected from sand bars or directly from stream channels. After washing and sieving, conventional magnetic separation techniques were applied to enrich quartz in the 0.125–0.5-mm grain size fraction. This grain size fraction was chosen, because it represents the dominant grain size of quartz in the exposed lithologies. This was followed by one etching step in 6 M HCl and several etching steps in diluted HF/HNO₃ in a heated ultrasonic bath to obtain pure quartz (cf. Kohl and Nishiizumi 1992). After dissolution of ~35 g quartz, Be was separated by successive solvent extractions, precipitated as Be(OH)₂ and transformed to BeO at 1,000°C. Following mixing of the BeO with copper powder for target preparation, the ¹⁰Be analysis was carried out at the AMS facility of ETH Zurich (details of the AMS measurements are given in Synal et al. 1997).

Quantification of erosion rates

In calculating erosion rates from the ¹⁰Be concentrations, we have followed the approach described by Schaller et al. (2002). Hence, erosion rates determined in this study will be easily comparable with erosion rates previously determined for central Europe (Schaller et al.

Fig. 2 Geological map of the Aabach catchment with erosion rates derived from cosmogenic ^{10}Be concentrations, river loads, and sediment trapped in reservoirs (for location see Fig. 1)

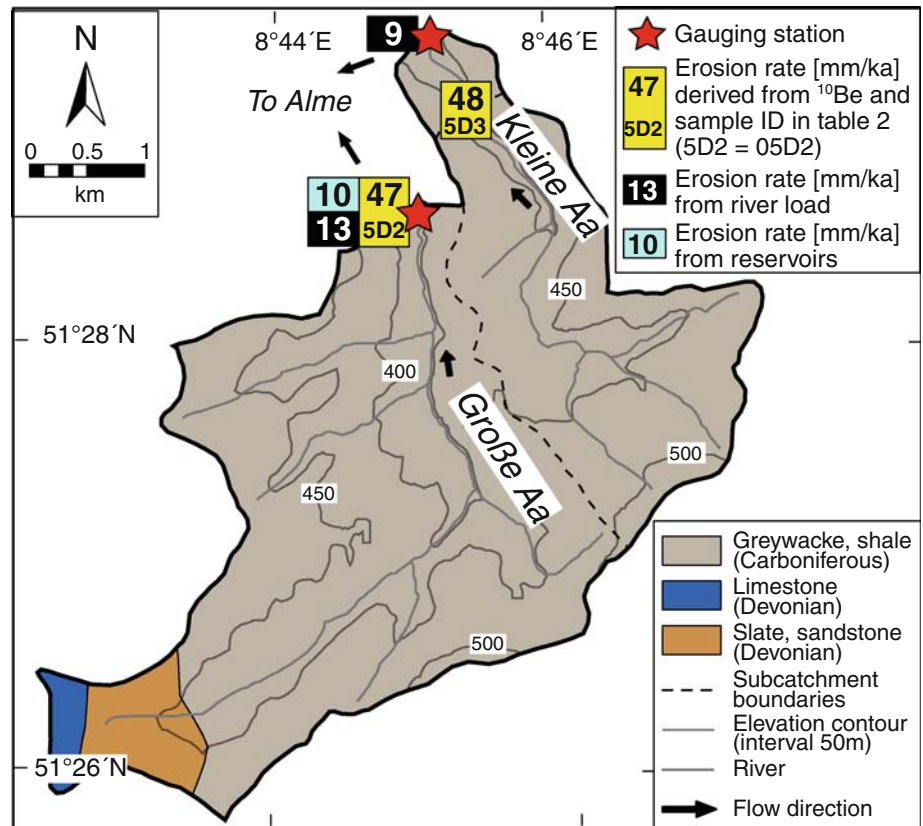
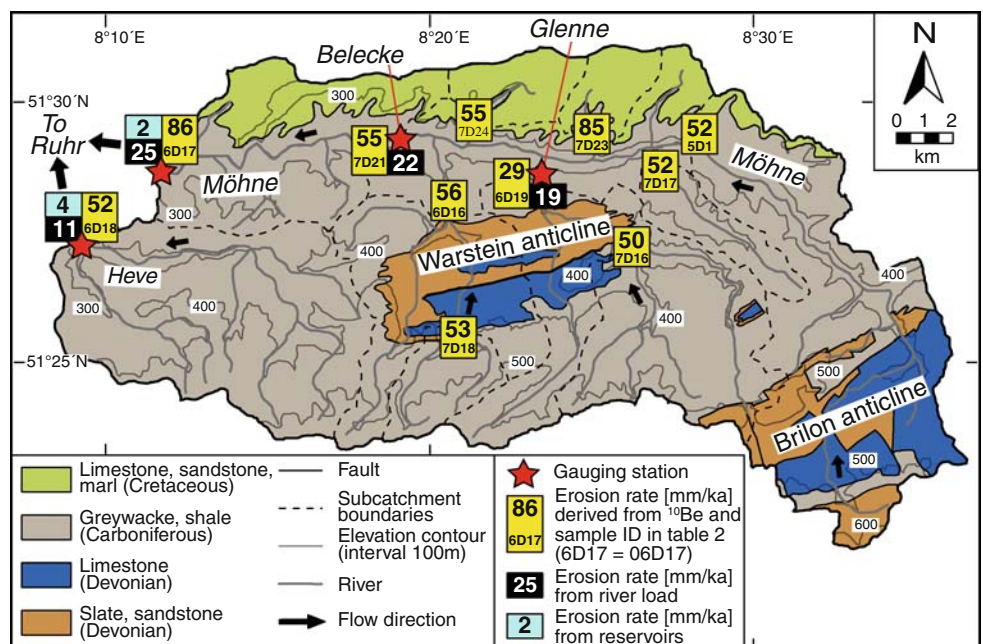


Fig. 3 Geological map of the Möhne catchment with erosion rates derived from cosmogenic ^{10}Be concentrations, river loads, and sediment trapped in reservoirs (for location see Fig. 1)



2001; Morel et al. 2003; Wittmann et al. 2007). Schaller et al. (2002) explicitly consider the ^{10}Be production by muons, which is important because, although ^{10}Be is predominantly produced by neutrons at the Earth's surface, the relative contribution of muons increases with depth and eventually becomes dominant (e.g., Gosse and

Phillips 2001). As a consequence, neglecting the ^{10}Be production by muons leads to an underestimation of erosion rates, which for the Rhenish Massif would be up to 25% lower (cf. Brown et al. 1995b; Balco et al. 2008). Schaller et al. (2002) used ^{10}Be production rates by neutrons, stopped muons, and fast muons at sea level and

Table 1 Location of gauging stations and data on precipitation, water discharge, evapotranspiration, and land use in the Aabach and Möhne catchments (Rhenish Massif, Germany)

Gauging station	Location		Basin area ^a (km ²)	Precipitation ^b (mm/a)	Discharge ^c (m ³ /s)	Acquisition period	Evapotranspiration ^d (mm/a)	Land use ^e (%)			
	Lat. 51°N	Long. 8°E						Forest	Pasture	Farmland	Urban area
Aabach catchment											
Große Aa	28'34"	45'00"	15.4	1,041	0.21	2002–2007	611	70.6	23.8	3.2	2.4
Kleine Aa	29'22"	45'04"	8.1	1,041	0.09	2003–2007	691	100.0	0.0	0.0	0.0
Möhne catchment											
Glenne	28'52"	23'25"	85.3	971	1.15	1959–2007	546	66.8	4.8	25.9	2.5
Belecke	29'11"	18'22"	328.8	978	4.06	1964–2007	589	51.0	10.2	31.1	7.7
Möhne	28'33"	11'40"	378.6	978	4.51	1960–2007	602	51.3	9.2	30.6	8.9
Heve	27'20"	09'20"	85.1	1,047	1.09	1960–2007	643	86.0	3.0	9.8	1.2

^a Basin areas were determined from 90 m SRTM digital elevation data

^b Mean precipitation measured by the water agencies *Aabach-Talsperre* and *Ruhrverband*, and by *Deutscher Wetterdienst*

^c Mean discharge measured by the water agencies *Staatliches Umweltamt Lippstadt*, *Aabach-Talsperre*, and *Ruhrverband* during the specified acquisition periods

^d Evapotranspiration was calculated by subtracting the discharge from the precipitation, taking into account the basin area

^e Land use is based on the Corine Land Cover map 2000 of the European Environment Agency (EEA[®], Copenhagen, EEA 2000; <http://www.eea.eu.int>)

high latitude ($\geq 60^\circ$) of 5.33, 0.106, and 0.093 at/g/a, respectively, which are based on the total ^{10}Be production rate determined by Kubik et al. (1998) and data on muon production (Heisinger et al. 2002a, b). Using the scaling model of Dunai (2000), we adjusted these production rates separately to the mean latitude and mean altitude of the different subcatchments studied here. Topographic parameters were determined from digital elevation Shuttle Radar Topography Mission (SRTM) data with a spatial resolution of 90 m. Quantification of topographic shielding using the algorithm of Codilean (2006) indicates that shielding is negligible (shielding factors for all catchments >0.999 , i.e., close to 1). The erosion rates calculated for the Aabach and Möhne catchments range from 29.4 ± 1.9 to 86.4 ± 6.4 mm/ka (Table 2). We report two different errors: the first one only includes the analytical error (1σ) of the AMS measurement, whereas the second one takes into account an estimated uncertainty on the total ^{10}Be production rate of 10%. The first error is appropriate for inter-sample comparison, but the second one should be used when comparing results from this study with erosion rates determined by other methods.

Short-term erosion rates derived from river loads

Sample collection and preparation

For quantification of dissolved loads, rivers were sampled twice at all six gauges in autumn 2006 at low discharge and

in spring 2007 at high discharge. The pH was measured in the field, whereas HCO_3^- was quantified via acid titration within 24 h after sampling. Selected dissolved constituents were analyzed with ICP-OES (Na^+ , K^+ , Mg^{2+} , Ca^{2+} , Si^{4+}) and ion chromatography (SO_4^{2-} , Cl^- , NO_3^-). For carbon isotope analyses of dissolved inorganic carbon (DIC), water samples were poisoned with HgCl_2 and closed air-tight in the field. Mass spectrometric measurements were performed using a ThermoFinnigan Delta Plus XL coupled to a GasBench II. The $\delta^{13}\text{C}$ values are reported in permil relative to V-PDB. In general, only mean values are reported for the dissolved load from both sampling periods (Table 3).

The suspended load in rivers is strongly dependent on discharge. Representative sampling for quantifying the suspended load at different discharges was achieved by collecting 5–10 samples at each gauging station between autumn 2006 and autumn 2007. Emphasis was placed on high-discharge events, when the suspended load is expected to reach maximum values. As the water agencies measure the discharge every 15 min, it is well defined for the sampling periods. The amount of suspended load was determined by filtering 1 l of each water sample through a 0.45- μm filter.

Correcting for contributions not related to natural rock weathering

The dissolved river load results not only from the chemical weathering of bedrock, but comprises additional natural

Table 2 Sample locations, catchment characteristics, and erosion rates based on cosmogenic ^{10}Be in quartz from stream sediment from the Aabach, Möhne and Heve subcatchments (Rhenish Massif, Germany)

Sample	Location		Grain size (mm)	Basin area ^a (km ²)	Mean altitude ^a (m)	Mean hillslope ^a (°)	$^{10}\text{Be}^b$ (10^3 at/g)	Erosion rate (mm/ka)	Error ^c (mm/ka)	Total error ^d (mm/ka)
	Lat. 51°N	Long. 8°E								
Aabach subcatchments										
05D2	28'13"	45'04"	0.125–0.5	15.4	449	4.7	140.9 ± 8.5	46.7	± 3.0	± 5.5
05D3	29'01"	45'23"	0.125–0.5	7.0	447	4.1	138 ± 24	47.7	± 8.8	± 10
Möhne subcatchments										
05D1	29'07"	28'24"	0.125–0.5	98.8	443	5.4	102 ± 19	65	± 13	± 14
06D16	28'04"	20'32"	0.125–0.5	61.6	411	5.4	114.8 ± 6.6	56.1	± 3.4	± 6.5
06D17	28'33"	11'40"	0.125–0.5	378.6	393	5.1	74.5 ± 5.3	86.4	± 6.4	± 11
06D19	28'52"	23'25"	0.125–0.5	85.3	435	5.8	217 ± 13	29.4	± 1.9	± 3.5
07D16	27'25"	26'07"	0.125–0.5	50.4	452	5.7	133 ± 11	49.6	± 4.2	± 6.5
07D17	28'58"	26'53"	0.125–0.5	13.6	400	5.4	116.0 ± 6.2	55.0	± 3.1	± 6.3
07D18	25'36"	20'57"	0.125–0.5	14.3	480	6.3	127.8 ± 6.1	52.8	± 2.7	± 5.9
07D21	29'11"	18'50"	0.125–0.5	323.7	410	5.2	117.3 ± 7.0	54.8	± 3.4	± 6.4
07D23	28'57"	25'05"	0.125–0.5	10.9	345	2.9	73.5 ± 4.6	84.6	± 5.5	± 10
07D24	29'10"	21'10"	0.125–0.5	13.4	323	2.7	110.2 ± 6.7	54.8	± 3.5	± 6.5
Heve subcatchment										
06D18	27'20"	09'20"	0.125–0.5	85.1	387	5.5	122.0 ± 7.6	51.7	± 3.4	± 6.2

^a Basin areas, mean altitudes and mean hillslopes were determined from 90 m SRTM digital elevation data

^b ^{10}Be concentration with analytical error (1σ)

^c Analytical error (1σ) for inter-sample comparison

^d Combined analytical and estimated production rate error of 10% for inter-method comparison

and anthropogenic inputs. These must be subtracted from the total dissolved load in order to determine short-term erosion rates (Table 3).

A correction has been applied for the contribution of HCO_3^- in weathering solutions derived from the oxidation of soil organic matter. For this, the carbon isotopic composition of dissolved inorganic carbon (Table 3) was measured. In general, soil organic matter reflects plant debris (litter). The organic carbon stems from photosynthetic carbon fixation and is characterized by a $\delta^{13}\text{C}$ of about -25‰ (Buhl et al. 1991). Pure oxidation of this organic matter will not be accompanied by an isotope fractionation. However, dissolution of CO_2 in water causes a fractionation of about $+7\text{‰}$ (Wigley et al. 1978), ultimately leading to respective $\delta^{13}\text{C}_{\text{DIC}}$ values of about -18‰ . In contrast, carbonate rocks typically have $\delta^{13}\text{C}$ values of about 0‰ (Kendall and Doctor 2003). Hence, the proportion of HCO_3^- in river water derived from soil organic matter oxidation can be calculated as:

$$[\text{HCO}_3^-]_{\text{SOC}} = [\text{HCO}_3^-]_{\text{Tot}} \times \left(\frac{\delta^{13}\text{C}_{\text{DIC}}}{\delta^{13}\text{C}_{\text{SOC}} - \delta^{13}\text{C}_{\text{Carb}}} \right) \quad (1)$$

where $[\text{HCO}_3^-]_{\text{Tot}}$ is the total HCO_3^- concentration in river water, $\delta^{13}\text{C}_{\text{DIC}}$ is the measured carbon isotopic

composition of the total HCO_3^- , $\delta^{13}\text{C}_{\text{SOC}}$ is the carbon isotope value for DIC derived from oxidation of soil organic carbon (-18‰) (Buhl et al. 1991), and $\delta^{13}\text{C}_{\text{Carb}}$ is the carbon isotopic composition of exposed carbonate rocks (0‰) (Kendall and Doctor 2003). Applying this equation indicates that 50–66% of the total HCO_3^- in the streams of the Möhne and Aabach catchments originates from soil solutions (Table 3).

Another contribution to the dissolved river load stems from precipitation and its chemical inventory. Quantification for this atmospheric input was achieved by using respective data from Beilke et al. (2003) who determined the chemical composition of precipitation over Germany. For the control station Hilchenbach in the Rhenish Massif (for location see Fig. 1), the total concentration of solutes amounts to 4.6 mg/l. The final contribution to the dissolved river load, however, is affected by evapotranspiration causing an increase in concentration. For the six subcatchments upstream of the gauges, the water balance indicates that 56–66% of the precipitation is lost by evapotranspiration. To correct for the associated increase of solutes in surface waters, we calculated a mean evapotranspiration factor F_{ET} for the entire study area according to Négrel et al. (1993):

Table 3 Dissolved load concentration, pH value, and carbon isotopic composition of dissolved inorganic carbon from rivers in the Möhne and Aabach catchments (Rhenish Massif, Germany)

Gauging station	Na ⁺ (μmol/l)	K ⁺ (μmol/l)	Mg ²⁺ (μmol/l)	Ca ²⁺ (μmol/l)	SiO ₂ (μmol/l)	HCO ₃ ⁻ (μmol/l)	SO ₄ ²⁻ (μmol/l)	Cl ⁻ (μmol/l)	NO ₃ ⁻ (μmol/l)	∑Cations (μeq/l)	∑Anions (μeq/l)	NICB ^a (%)	pH	δ ¹³ C _{DIC} (‰) PDB
Total dissolved load														
Aabach catchment														
Große Aa	393	48	274	471	61	1,100	213	210	65	1,931	1,800	3.5	7.6	-12.0
Kleine Aa	341	40	269	367	54	925	185	136	37	1,654	1,468	5.9	7.4	-11.3
Möhne catchment														
Glenne	397	36	184	1,105	50	1,674	188	354	123	3,010	2,528	8.7	8.0	-11.8
Belecke	1,645	71	247	1,208	36	2,299	226	1,526	135	4,624	4,412	2.3	8.1	-11.5
Möhne	2,210	99	259	1,339	52	2,874	242	1,861	232	5,506	5,452	0.5	8.2	-11.8
Heve	279	30	179	297	61	550	169	215	64	1,261	1,167	3.9	7.2	-9.0
Dissolved load corrected for atmospheric and anthropogenic inputs														
Aabach catchment														
Große Aa	184	44	268	460	61	370	174	0	0	1,684	717			
Kleine Aa	207	37	263	356	54	347	147	0	0	1,482	640			
Möhne catchment														
Glenne	44	33	177	1,094	50	581	149	0	0	2,620	880			
Belecke	120	67	240	1,197	36	830	187	0	0	3,063	1,205			
Möhne	351	96	253	1,328	52	990	203	0	0	3,609	1,397			
Heve	65	27	173	286	61	276	130	0	0	1,010	537			

All values are averages of two samples collected in autumn 2006 and spring 2007

^a NICB = normalized inorganic charge balance, $[(\sum \text{cations} - \sum \text{anions}) / (\sum \text{cations} + \sum \text{anions})] \times 100$

Table 4 Erosion rates derived from river load gauging data for six subcatchments of the Aabach and Möhne catchments (Rhenish Massif, Germany)

Gauging station	Total dissolved load ^a (mg/l)	Atmospheric input ^b (mg/l)	Anthropogenic input ^c (mg/l)	Corrected dissolved load ^d (mg/l)	Suspended load ^e (mg/l)	Estimated bedload ^f (mg/l)	Total erosion rate ^g (mm/ka)	Erosion rate from suspended and bedload only ^g (mm/ka)
Aabach catchment								
Große Aa	139.1	56.2	9.1	73.8 ± 14.8	7.0 ± 2.1	1.0 ± 0.5	13.0 ± 2.4	1.3 ± 0.3
Kleine Aa	115.3	47.0	3.0	65.4 ± 13.1	4.7 ± 1.4	0.7 ± 0.4	9.2 ± 1.7	0.7 ± 0.2
Möhne catchment								
Glenne	202.8	78.4	21.0	103.3 ± 20.7	16.9 ± 5.1	2.5 ± 1.3	19.3 ± 3.4	3.1 ± 0.8
Belecke	321.6	101.3	90.3	130.0 ± 26.0	16.3 ± 4.9	2.4 ± 1.2	21.5 ± 3.8	2.7 ± 0.7
Möhne	396.8	126.7	115.9	154.2 ± 30.8	23.9 ± 7.2	3.6 ± 1.8	25.3 ± 4.4	3.8 ± 1.0
Heve	88.9	28.4	9.2	51.3 ± 10.3	19.2 ± 5.8	2.9 ± 1.4	11.0 ± 1.8	3.3 ± 0.9

^a Mean dissolved load concentrations from measurements in autumn 2006 and spring 2007

^b Including HCO_3^- from the oxidation of organic matter

^c Including NaCl groundwater from the river water of the gauging stations Belecke and Möhne

^d Dissolved load corrected for atmospheric and anthropogenic input. Assumed error, 20%

^e Suspended load corrected for organic input. Assumed error, 30%

^f Assumed error, 50%

^g Rock density in the catchments is assumed to be 2.7 g/cm³

$$F_{\text{ET}} = \frac{\sum_{i=1}^n P_i}{\sum_{i=1}^n \frac{Q_i}{A_i}} \quad (2)$$

where P_i is the precipitation, Q_i is the discharge, and A_i is the area of the respective watersheds (Table 1). Note that groundwater discharge has been neglected in this water balance, and therefore, the value for F_{ET} of 2.56 is a maximum estimate. Subsequently, we multiplied the concentration of solutes in the precipitation by 2.56 and subtracted these evapotranspiration-corrected concentrations from the total dissolved load (Table 3). As the factor F_{ET} is a maximum estimate, the non-atmospheric dissolved loads are minimum values. In summary, the total atmospheric inputs, including the contribution of HCO_3^- from oxidation of organic matter, in the respective subcatchments vary from 28 to 127 mg/l, which is equivalent to 31–41% of the total dissolved load (Table 4).

Anthropogenic pollution constitutes another input source that needs to be corrected for when determining the natural dissolved load in rivers. In general, the amount of dissolved load in rivers is considerably higher in urban areas compared to sparsely populated regions (Flintrop et al. 1996). In the Möhne and Aabach catchments, the total dissolved river loads increase with the proportion of farmland and urban areas (Fig. 4). Higher dissolved loads, especially in the subcatchments having a high percentage of farmland, are influenced by anthropogenic inputs. Likely, all NO_3^- is ultimately derived from agriculture and was subtracted from the measured total dissolved load (Table 3).

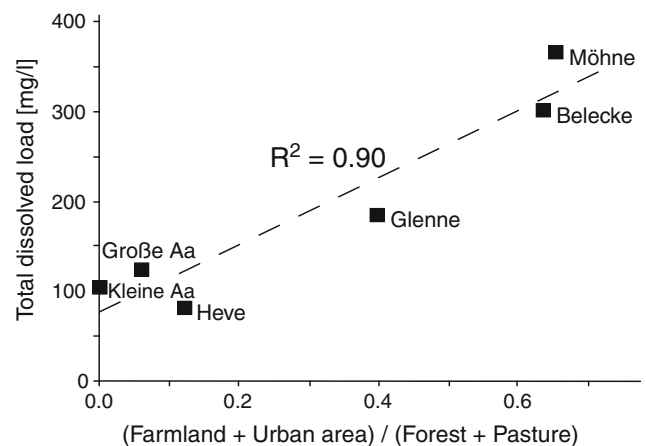


Fig. 4 Relationship between total dissolved loads and land use, described as the ratio between farmland and urban area divided by the area with forest and pasture, for the subcatchments of the six gauging stations. The four land use categories are given in Table 1

In addition to atmospheric inputs, Cl^- in river water originates from weathering of evaporites and/or from direct anthropogenic inputs (e.g., Roy et al. 1999). In the absence of evaporites in a given catchment, Cl^- is commonly used to identify the magnitude of anthropogenic pollution (e.g., Négrel et al. 1993). No evaporites are exposed in the studied areas, hence, no direct contribution from evaporite dissolution can be expected. However, from the western part of the Warstein anticline, situated within the Möhne catchment, groundwater is delivering NaCl to the Westerbach stream (Fig. 3) (Koch et al. 1974). Very likely, this contribution is causing the increased Na^+ and Cl^-

concentrations at the gauges Belecke and Möhne (Table 3). The NaCl-containing groundwater originates in the Brilon anticline, where streams trickle away in the karst (Busch and Ewald 2000). We assume that after correcting for the input from precipitation, the remaining Cl^- is derived from NaCl-rich groundwater and from anthropogenic sources such as communal and industrial effluents, i.e., road salts and fertilizers. Similarly, Na^+ is a dominant pollution ion (Flintrop et al. 1996). Hence, after correcting for the atmospheric contribution, the remaining Cl^- and the stoichiometric proportion of Na^+ are subtracted from the dissolved river loads. We acknowledge that this is still a rather simplified correction, as other major ions in addition to Na^+ could result from anthropogenic inputs, such as K^+ , Mg^{2+} and Ca^{2+} commonly present in fertilizers.

For two reasons, the applied correction for anthropogenic inputs leads to geogenic dissolved loads that are maximum estimates. First, the difficulty to identify all anthropogenic sources may underestimate the anthropogenic inputs. Second, anthropogenic inputs such as SO_4^{2-} and NO_3^- , which decrease the pH value in soils, lead to increased chemical weathering (Drever 1994). The anthropogenic inputs in the six watersheds, including the contribution of NaCl from groundwater, constitute 3–116 mg/l or 3–29% of the total dissolved river load (Table 4). Thereby, the rivers within the Belecke and Möhne subcatchments show the highest proportions of anthropogenic pollution, because they receive NaCl-rich groundwater.

Following all applied corrections, the dissolved river loads considered to result exclusively from rock weathering range from 51 to 154 mg/l or 39–58% of the measured total dissolved loads (Table 4). Still, the concentrations of Ca^{2+} and HCO_3^- in the three watersheds of the Möhne (Glenné, Belecke, and Möhne in Table 3) are higher than in the Heve subcatchment and the two subcatchments of the Aabach catchment. These high concentrations of Ca^{2+} and HCO_3^- are presumably a consequence of the Devonian limestones exposed in the Warstein and Brilon anticlines and exposed Cretaceous carbonates north of the Möhne valley (Fig. 3). Corrected dissolved loads are reported with an estimated uncertainty of $\pm 20\%$ (Table 4).

Determination of suspended load and estimation of the bedload

In general, the amount of suspended load is positively correlated with discharge, and infrequent flood events may transport large amounts of sediment (e.g., Schmidt and Morche 2006). This is also apparent in the present data set, as suspended loads during high-discharge events are more

than one order of magnitude higher than during low discharge (Fig. 5). In order to quantify this relationship, regression analysis using either polynomial or power functions were performed (Fig. 5). Applying these functions, we calculated time-integrated suspended loads in milligram per liter (SPM_{Poly} for polynomial functions and SPM_{Pow} for power functions) within the respective periods of 5–49 years during which discharge has been monitored (Table 1):

$$\text{SPM}_{\text{Poly}} = \frac{\sum_{i=1}^n Q_i \times (a \times Q_i^2 + b \times Q_i)}{\sum_{i=1}^n Q_i} \quad (3)$$

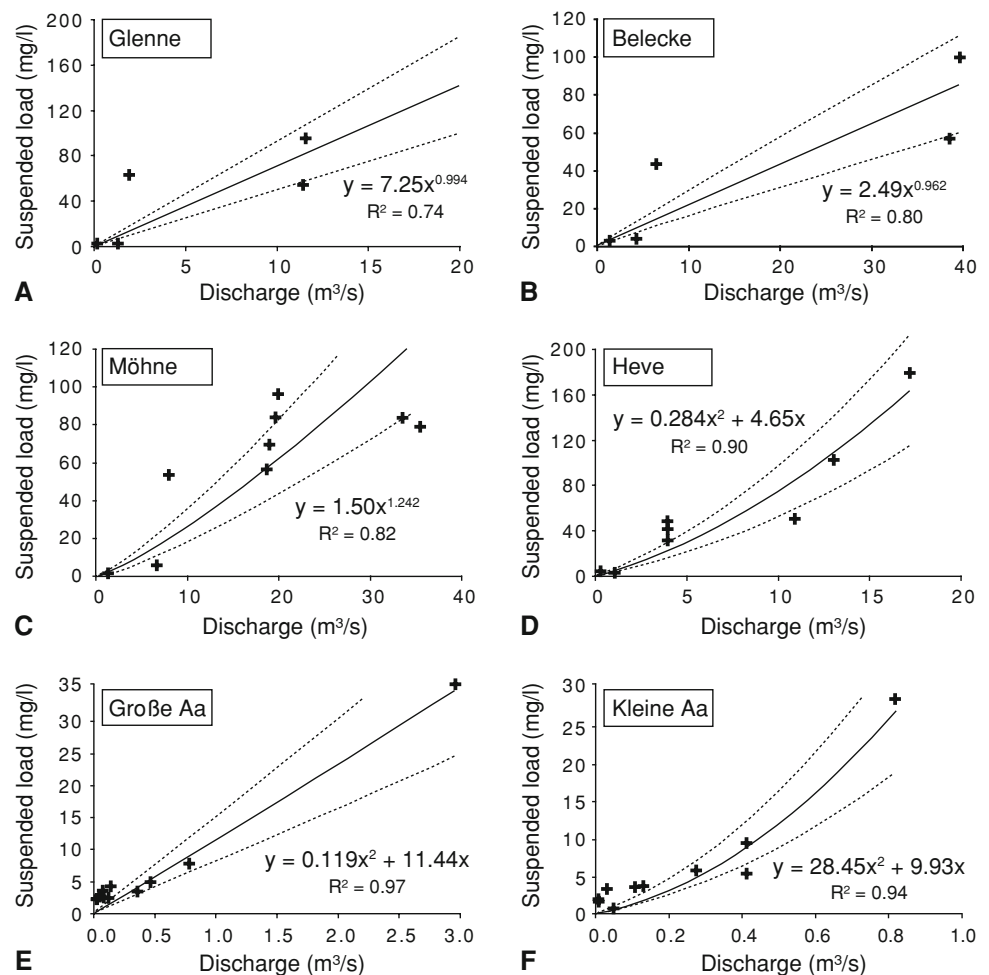
$$\text{SPM}_{\text{Pow}} = \frac{\sum_{i=1}^n Q_i \times (a \times Q_i^b)}{\sum_{i=1}^n Q_i} \quad (4)$$

where n is the number of days since the water agencies started to record discharge, Q_i is the daily mean discharge, and a and b are coefficients from the respective rating curves (Fig. 5). The suspended loads must be corrected for modern particulate organic matter in order to quantify the suspended river load solely derived from rock weathering. Kaspar (1993) determined this organic component in a river of comparable size draining a low mountain range in southern Germany. She concluded that organic matter accounts for 5–30% of the suspended load, depending on the season and vegetation cover. We applied an average value of 15% organic matter for correcting the suspended river loads, resulting in a range of 5–24 mg/l for the Möhne and the Aabach. For all six gauges, the corrected suspended loads are considerably smaller than the dissolved loads (Table 4).

In general, the sediment peak during individual high-discharge events commonly precedes the peak discharge and follows a clockwise hysteresis loop (Lenzi and Marchi 2000; Rovira and Batalla 2006). Owing to the individual characteristics and location of active sediment sources in different catchments, as well as the variable time interval during two subsequent high-discharge events, the relationship between suspended load and discharge is often more complex (Lenzi and Marchi 2000). Therefore, we estimate an uncertainty of $\pm 30\%$ for the suspended loads (Table 4; Fig. 5).

In general, bedload transport in streams occurs within well defined hydrographic thresholds, however, a well-established formula for calculating the bedload is lacking (Rickenmann 1997; Martin 2003). Many studies in low mountain ranges consider a value of 10% of the total suspended load in order to approximate bedload (e.g., Judson and Ritter 1964; Summerfield and Hulton 1994). Kaspar (1993) determined comparable values of 10–20% for the bedload in a river draining Jurassic mudstones, whereas in a granitic watershed the bedload amounted to 40–50% of the suspended load. As the Möhne and Aabach

Fig. 5 Relationship between discharge and suspended load for the gauging stations of the Möhne subcatchments (a–d) and the Aabach subcatchments (e–f). The best fitting trend lines for this relationship, either polynomial functions (a–c) or power functions (d–f) are shown as *solid lines* with the respective equations. The *dotted lines* represent an estimated uncertainty for the suspended load of $\pm 30\%$



catchments drain very low grade to unmetamorphosed sedimentary rocks, we estimate the bedload to be 15% of the suspended load and assume an error of 50% (Table 4) to account for the bedload range observed previously in sedimentary rocks (e.g., Kaspar 1993).

For converting the concentrations of the different river loads to total erosion rates [mm/ka], we considered a bedrock density of 2.7 g/cm^3 , the respective basin areas, and the discharge recorded by the six gauging stations over periods between 5 and 49 years. These short-term erosion rates of the Aabach and Möhne catchments range from 9 to 25 mm/ka (Table 4).

Discussion

Comparison of long-term and short-term erosion rates in the Rhenish Massif

The long-term erosion rates derived from cosmogenic ^{10}Be concentrations of stream sediments in the Aabach and Möhne catchments are very homogenous and range from

46.7 ± 5.5 to $65 \pm 14 \text{ mm/ka}$, with the exception of three samples to be discussed below (Table 2; Figs. 2, 3). The determination of erosion rates with ^{10}Be is potentially complicated by the storage and remobilization of sediments, because during storage additional ^{10}Be is generated near the surface, whereas ^{10}Be is lost due to radioactive decay, if sediment is shielded at depth. However, the net effect on cosmogenic nuclide concentrations will be small as long as the mean residence time of the sediment in storage and transport is shorter than the time during which ^{10}Be is produced on the hillslopes (Granger et al. 1996). Long-term deposition of sediment and subsequent irradiation would result in a progressive downstream increase in the concentration of cosmogenic nuclides and a decrease of erosion rates (cf. Schaller et al. 2001). Such a downstream decrease in the erosion rates is not observed along the Möhne river and its tributaries (Fig. 3). Especially the high erosion rate of $86 \pm 11 \text{ mm/ka}$ recorded by sample 06D17 from the outlet of the Möhne catchment indicates that long-term deposition of sediment in the floodplain and subsequent irradiation does not play a detectable role. The Kitzelbach stream, draining a subcatchment containing a

large proportion of Cretaceous sediments at the northern margin of the Möhne catchment, also yields a relatively high erosion rate of 85 ± 10 mm/ka (sample 07D23). However, this likely reflects the presence of weakly consolidated Cretaceous sediments comprising alternating layers of sandstone, marl, and limestone (Clausen and Leuteritz 1984). In the Glenne subcatchment, a low erosion rate of 29.4 ± 3.5 mm/ka was recorded for sample 06D19. In principle, long-term storage and irradiation of sediment at a shallow depth of ≤ 2 m, possibly in karstified limestones of the Warstein anticline, could explain the high ^{10}Be concentration of this sample. However, a sample from the Westerbach stream, which traverses the Warstein anticline about 5 km farther to the west, yielded an erosion rate of 56.1 ± 6.5 mm/ka (sample 06D16), i.e., very similar to most other samples. Thus, the uniquely low erosion rate for the Glenne subcatchment remains unexplained at present.

Erosion rates determined with ^{10}Be integrate over the period that is required to remove about ~ 60 cm of bedrock with a density of 2.7 g/cm^3 or an equivalent mass of less dense soil, which is present in the investigated catchments. For the investigated catchments this is a period of 9–13 ka. As cosmogenic nuclides are quite insensitive to short-term changes in erosion rate, i.e., to temporal violations of the steady-state assumption, they should provide a robust estimate of the natural background erosion rates (von Blanckenburg 2006). Consequently, the ^{10}Be -based erosion rates determined here should not reflect any recent changes in land use. This is quite variable at present, for example, the subcatchment of the Kleine Aa is completely forested, whereas the Möhne subcatchments comprise 30% farmland and only 50% of forest cover (Table 1). Despite these pronounced differences the long-term erosion rates in the Möhne and Aabach watersheds do not show any correlation with land use; a conclusion that is comparable to previous studies in other climatic settings (Hewawasam et al. 2003; von Blanckenburg 2006; Vanacker et al. 2007). In addition,

the ^{10}Be erosion rates are also independent of catchment size.

The short-term erosion rates derived from the river loads in the Aabach and Möhne catchment integrate over the period for which discharge data are available, i.e., between 5 and 49 years (Table 1). The samples collected at the two gauging stations in the Aabach catchment and the Heve subcatchment yield similar erosion rates between 9 and 13 mm/ka. In contrast, river loads from the Glenne, Bel-ecke, and Möhne subcatchments are about twice as high, resulting in erosion rates of 19–25 mm/ka (Table 4). This difference is most likely caused by limestone exposures in the Warstein and Brilon anticlines of the Möhne catchment (Fig. 3) that are affected more strongly by chemical weathering and contribute large amounts of Ca^{2+} and HCO_3^- to the dissolved load (Table 3). The volumes of sediment trapped in three storage basins located in front of the reservoirs of the Möhne and Aabach catchments provide an independent check for the erosion rates derived from river loads over periods of 13, 16, and 28 years, respectively (Table 5). However, when comparing these two data sets it must be kept in mind that the sediments in the storage basins reflect only the sum of suspended and bedload, but do not account for the dissolved load. Consequently, the erosion rates calculated from the sediment storage are expected to be considerably lower than the rates derived from river load data. More precisely, the reservoir-based erosion rates should mirror those determined from the suspended and the bedload. This is seen for the reservoirs in the Möhne and Heve subcatchments, with respective erosion rates of ~ 2 and ~ 4 mm/ka, compared to ~ 25 and ~ 11 mm/ka, respectively (Tables 4, 5). For the subcatchment of the Große Aa, however, the erosion rates determined from sediment storage, i.e., ~ 10 mm/ka, and based on river load, ~ 13 mm/ka, are nearly identical. The large volume of sediment deposited in the Aabach storage basin between 1983 and 1996 results from higher suspended load and bedload fluxes than today. The strong

Table 5 Erosion rates based on the volume of sediment in reservoirs of the Aabach and Möhne catchments (Rhenish Massif, Germany)

Reservoir	Basin area ^a (km ²)	Volume of sediment ^b (m ³)	Period of observation (a)	Accumulation rate of sediment (m ³ /a)	Erosion rate ^c (mm/ka)
Aabach catchment					
Große Aa	16.6	4,700	1983–1996	362	10.3
Möhne catchment					
Möhne	398.3	21,760	1982–1998	1,360	1.6
Heve	118.5	26,132	1969–1997	933	3.7

^a Basin areas were determined from 90 m SRTM digital elevation data

^b Volumes of sediment measured by the water agencies *Aabach-Talsperre* and *Ruhrverband*

^c To convert the sediment volume deposited in the reservoir to an erosion rate we used a density of 1.5 g/cm^3 for the sediments in the reservoirs. The organic fraction buried with the trapped sediment was assumed to be 15%

decrease of the particulate loads over the two decades since the completion of the Aabach dam in 1983 can be explained by reforestation measures that were undertaken to reinforce the river banks (Milde 1996). In summary, the erosion rates derived from the amount of sediment stored in the reservoirs of Aabach and Möhne agree with the erosion rates from respective river loads that integrate over approximately the same time period. The conformity of both results suggests that increased export of suspended load and bedload during flood events in the past decades is appropriately captured by the rating curves used to calculate the short-term erosion rates (Fig. 5; Table 4). Nevertheless, short-term erosion rates derived from river loads in the Möhne and Aabach watersheds are only about one-third of the erosion rates derived from cosmogenic nuclides (Tables 2, 4). In the next section we suggest possible reasons for this discrepancy.

Discrepancy between short- and long-term erosion rates

Several authors have argued that rare flood events, which are not captured in the relatively short acquisition period of discharge data, are responsible for higher long-term erosion rates as compared to short-term erosion rates (cf. Schaller et al. 2001; Kirchner et al. 2001; Ferrier et al. 2005). In this section we performed two model simulations to explore if flood events or higher average rates of precipitation can explain the discrepancy between the erosion rates on different timescales. In both simulations, we assumed that the mismatch is entirely caused by the low amount of the particulate load (suspended load and bedload). For both model simulations, we used the rating curves relating discharge and suspended load (Fig. 5) to calculate by how much the discharge has to be increased in order to raise the short-term erosion rates to the average long-term rate recorded with ^{10}Be (~ 57 mm/ka). In the simulations the concentration of the dissolved load is held constant, because the degree of chemical weathering does not depend on the annual precipitation (Riebe et al. 2004). Because discharge data for the Aabach catchment are only available for the last few years, we restricted the models to the four subcatchments of the Möhne watershed for which discharge data are available for the last 44–49 years (Table 1). In the following, we explain both model simulations in detail.

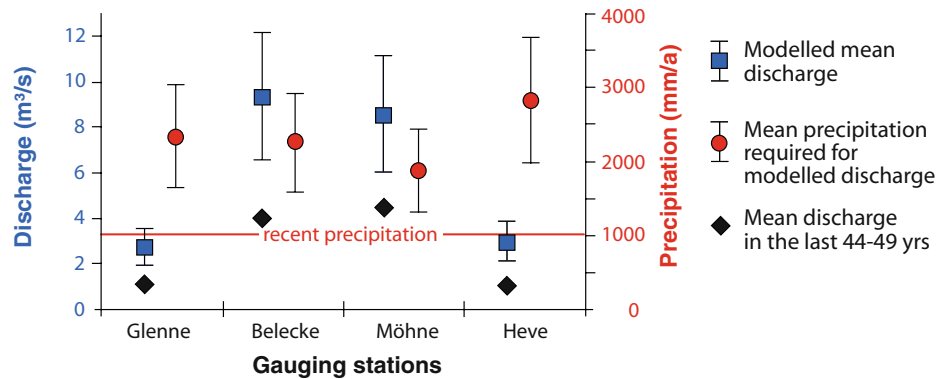
In the first model, the daily mean discharge is increased over the entire duration of the model run (44–49 years). This simulation shows that in order to attain short-term erosion rates of 57 mm/ka by increasing the solid load, the mean discharge must be 1.9–2.7 times higher than the measured discharge. All other factors being equal, this implies an average precipitation during the Holocene of 1,900–2,800 mm/a, which is about two to three times

higher than the present-day precipitation of about 1,000 mm (Fig. 6a). Given that climate conditions in the Holocene have been relatively stable, the very high precipitation values required imply that the discrepancy between short- and long-term erosion rates cannot be explained by a higher precipitation in the past.

The second model assumes that most of the solid load is transported out of the catchments during rare flood events. We simulated a single flood with highly elevated discharge lasting 1 week to increase the solid load such that the short-term erosion rates in the four subcatchments attain the long-term erosion rate of ~ 57 mm/ka. The required discharges are 4–17 times higher than the maximum discharges during the respective measured periods (44–49 years) and range from 140 to 900 m^3/s (Fig. 6b). Note, that in order to balance short-term and long-term erosion rates, a flood of the simulated size would have to occur once every four to five decades. Such a high frequency of flood events exceeding the magnitude of events recorded in the last 4–5 decades by a factor of 4–17 is considered highly unlikely, especially in the light of stable environmental conditions during the mid-Holocene recorded by rather low sediment yields in Central Europe (Zolitschka 2002). In summary, the two model simulations suggest that the discrepancy between short-term and long-term erosion rates can only partly be explained by periods of increased discharge, due to a higher mean precipitation, and rare flood events.

Past variations in the erosion rate, i.e., a deviation from the steady-state assumption underlying the cosmogenic nuclide approach, could also contribute to the observed discrepancy between short-term and long-term erosion rates. This is illustrated by numerical models which simulate stepwise changes in the rate of erosion through time and show that the erosion rate recorded by ^{10}Be always lags the actual erosion rates by some time (Bierman and Steig 1996; von Blanckenburg 2006; Heimsath 2006). These models suggest that ^{10}Be concentrations may contain a signal of the earlier phase of more rapid erosion even thousands of years after a sudden drop in erosion rate. Indeed, such an elevated Late Pleistocene erosion signal has been inferred for the rivers Allier and Meuse from the ^{10}Be concentration in modern stream sediments and terrace deposits (Schaller et al. 2002). In the following, we describe some evidence for temporally changing erosion rates in the Rhenish Massif and other central European mountains.

A detailed analysis of varved sediments in Lake Holzmaar in the western Rhenish Massif has shown that sediment yield varied considerably during the last ~ 14 ka. For instance, during the Younger Dryas, the Roman Empire, and the Middle Ages sediment yields were more than twice as high as the average rate over the last 14 ka

A Model 1: Increase in annual discharge (and precipitation)**B Model 2: One huge flood every 5 decades**

Simulated floods have a duration of one week

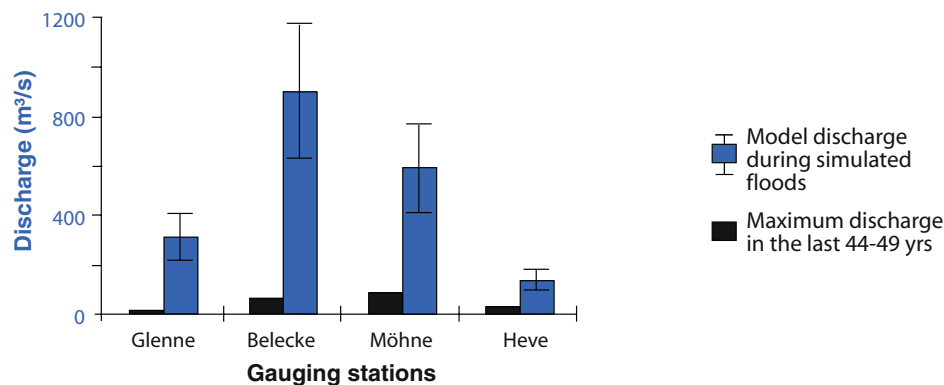


Fig. 6 Results of two model simulations that quantify the increase in discharge and precipitation required to increase short-term erosion rates (based on river loads) to the mean long-term erosion rate of ~ 57 mm/ka (derived from ^{10}Be). The models focus on four subcatchments of the Möhne watershed for which discharge data are available for the last 44–49 years (Table 1). Both models use the rating curves relating discharge and suspended load along with their estimated uncertainty of $\pm 30\%$ (Fig. 5). Hence, the required

discharge and precipitation values are shown with an uncertainty of $\pm 30\%$ for both models. **a** The first model assumes an increase of the mean annual discharge (shown in blue); the annual precipitation required to reach this higher discharge is shown in red. **b** The second model assumes a single flood event with a duration of 1 week. The required discharges of the simulated floods (shown in blue) are compared to the maximum discharges measured during the last 44 to 49 years

(Zolitschka 1998; 2002). The clearance of forests by the Romans and later in the Middle Ages destabilized soils and led to sheet erosion on hillslopes, which explains the high sediment yields during these periods (Zolitschka 1998). A decreasing evapotranspiration owing to deforestation may have increased surface runoff and provides a positive feedback mechanism on erosion (e.g., Bork et al. 1998). During the Younger Dryas cold phase the presence of tundra-like vegetation made soils more susceptible to erosion, while frozen ground inhibited infiltration during spring-time melting and also intensified erosion (Zolitschka 1998). A similar picture of increased sediment yield in the Middle Ages and the Younger Dryas emerges for the Lac Chambon watershed in the Massif Central (Macaire et al. 1997). In addition, higher erosion rates during the Younger Dryas and the last glacial maximum were presumably caused by the rapid down-slope

movement of periglacial cover deposits (cf. Matsuoka 1998), which were described in many parts of central Europe (e.g., Semmel 1968; Völkel 1995; AK Bodensystematik 1998). We suggest that the enhanced erosion rates during these prolonged cold periods and the associated lower ^{10}Be concentration of exhuming bedrock and regolith are still partly inherited today. Although the ^{10}Be -based erosion rates may therefore slightly overestimate the Holocene erosion rates, they should provide a reasonable constraint on the time-integrated erosion rate during the last glacial–interglacial cycle.

Comparison of erosion rates in the Rhenish Massif to other studies in central Europe

The comparison of the short-term erosion rates derived from river loads in the Rhenish Massif to other studies in

central Europe is hampered, because of different approaches that were used to correct for atmospheric and anthropogenic inputs and for quantifying the solid load (i.e., suspended + bedload). However, erosion rates for central Europe determined in a comparable way from river loads vary from 6 to 28 mm/ka (Roy et al. 1999; Schaller et al. 2001) and are generally lower than long-term erosion rates by a factor of about 2–7 (Fig. 7a). The short-term rate of ~ 16 mm/ka for the Meuse watershed, which is located in the western Rhenish Massif and drains similar sedimentary rocks as present in our study area, agrees well with the average erosion rate of $\sim 17 \pm 3$ mm/ka for the Aabach and Möhne catchments (Fig. 7b). The highest erosion rates of ~ 28 and ~ 26 mm/ka were reported for the Seine and Neckar catchments, which both contain a significant proportion of readily weathering carbonates. Catchments with crystalline rocks such as the Loire watershed and the Regen catchment, a small subcatchment of the Danube, yield significantly lower erosion rates of ~ 6 and ~ 7 mm/ka (Fig. 7a). This compilation supports our conclusion that short-term erosion rates are clearly dependent on the exposed lithology.

In order to allow for a direct comparison between erosion rates based on ^{10}Be , it is of crucial importance that different studies use the same procedures with respect to

scaling and muon contribution. Following Schaller et al. (2001, 2002) and Morel et al. (2003), our erosion rates for the Rhenish Massif can be directly compared to the ones reported in these studies (note that the original erosion rates in Schaller et al. (2001) were recalculated by Schaller et al. (2002), who first applied the approach that we also use here). To enable a simple comparison between these different studies, we calculated mean erosion rates and standard deviations for suites of samples from different river catchments (Fig. 7a). The mean erosion rate derived for the Aabach and Möhne catchments is 57 ± 15 mm/ka. Comparable erosion rates have been obtained for the large river basins of the Loire (43 ± 19 mm/ka) and the Meuse (36 ± 16 mm/ka) (Schaller et al. 2001, 2002). The Regen, which drains crystalline rocks, yielded a slightly lower erosion rate of 31 ± 3 mm/ka than the catchments in the Rhenish Massif. In contrast, the Neckar catchment containing many carbonates and evaporites displays a higher erosion rate of 100 ± 30 mm/ka (Schaller et al. 2001, 2002). The control of lithology on rates of erosion is also reflected by ^{10}Be data from the Black Forest, where the Wutach and the Danube watersheds yield mean erosion rates of 15 ± 4 mm/ka in areas with well-lithified Triassic sandstones and 51 ± 25 mm/ka in crystalline gneisses and granites (Morel et al. 2003) (Fig. 7a).

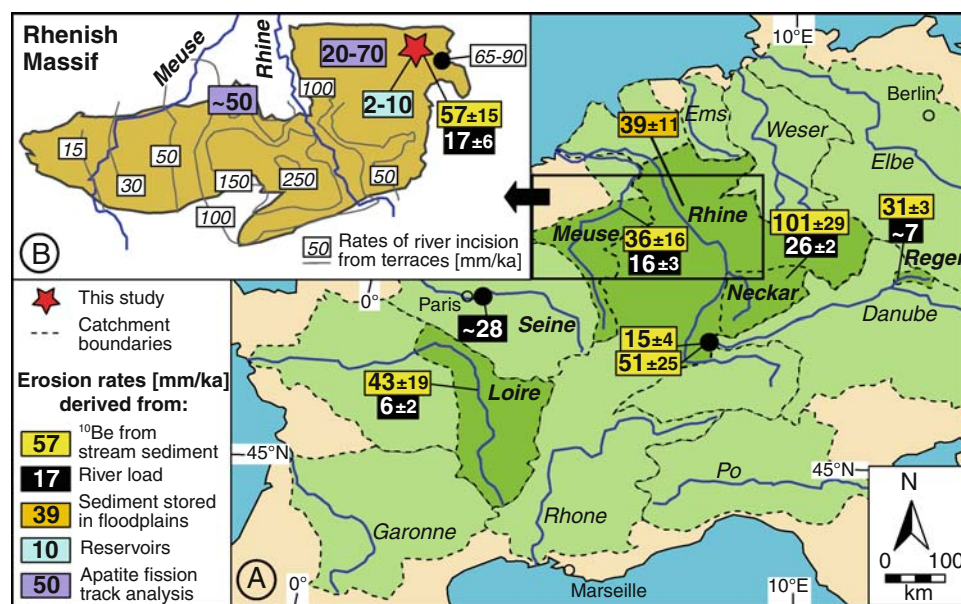


Fig. 7 Compilation of short and long-term erosion rates and rates of river incision in low mountain ranges of central Europe. Errors given for the ^{10}Be -based erosion rates are standard deviations calculated for several samples from the respective river catchments. **a** Erosion rates for the Loire, Meuse, Neckar, and Regen watersheds are from Schaller et al. (2001, 2002). The erosion rate values in SW Germany are reported by Morel et al. (2003) and refer to catchments with Triassic sandstones (15 ± 4 mm/ka) and Paleozoic crystalline rocks (51 ± 25 mm/ka), respectively. The short-term erosion rate of the Seine catchment is based on river load data (Roy et al. 1999), whereas

the long-term rate for the Rhine basin, without the Alps, has been determined from the volume of Holocene sediments stored in floodplains (Hoffmann et al. 2007). **b** Contour lines indicating rates of river incision in the Rhenish Massif were derived from river terraces (Meyer and Stets 1998; van Balen et al. 2000). The incision rate of 65–90 mm/ka in the northeastern part of the massif is based on terraces described by Wortmann (1937) and Meiburg (1979). Denudation rates obtained from apatite fission track analysis for regions west and east of the Rhine are from Glasmacher et al. (1998) and Karg et al. (2005), respectively. See text for further explanation

For the entire Rhine catchment, without the Alps, a Holocene erosion rate of 39 ± 11 mm/ka (Fig. 7a) has been estimated from the volume of sediment stored in floodplains and the delta (Hoffmann et al. 2007). Our ^{10}Be -based erosion rates for the two studied catchments range from 46.7 ± 5.5 to 65 ± 14 mm/ka (neglecting three values discussed above) are somewhat higher than the Holocene rate of Hoffmann et al. (2007), although they integrate over the same time period. For three reasons, the slight discrepancy is not surprising. First, the investigated catchments in the Rhenish Massif are located in a mountainous region of the Rhine catchment with a higher relief and slightly steeper slopes than the average subcatchments of the Rhine. Second, based on a sensitivity analysis and literature data Hoffmann et al. (2007) interpreted their erosion rate as minimum estimate. Third, a lower contribution of muons to the ^{10}Be production and a lower total ^{10}Be production rate as assumed in our approach would decrease our ^{10}Be erosion rates by 10–20%.

Implications for landscape evolution in central Europe

The long-term mean erosion rate 57 ± 15 mm/ka derived for the northeastern Rhenish Massif during this study is similar to the local rate of river incision of 65–90 mm/ka, roughly constrained by the five terrace levels along the Diemel (Wortmann 1937; Meiburg 1979) (Fig. 7b). Hence, if the rate of incision equals the rock uplift rate, then our ^{10}Be data imply a steady state between uplift and erosion in this part of the Rhenish Massif. A similar agreement between rock uplift, catchment-wide erosion, and river incision has recently been inferred for the Apennines over the last ~ 1 Ma (Cyr and Granger 2008).

Denudation rates on timescales of tens of million of years can be inferred from thermal modeling of track length distributions of fission tracks in apatite (e.g., Laslett and Galbraith 1996). Such data indicate that the northern Rhenish Massif east of the Rhine experienced denudation rates of about 20–70 mm/ka in the Mesozoic and Cenozoic (Karg et al. 2005). Accelerated cooling rates since the early Tertiary suggest that Cenozoic erosion rates were higher than those in the Mesozoic (Karg et al. 2005); probably in the range of 40–70 mm/ka. A similar average denudation rate of ~ 50 mm/ka since ~ 120 Ma has been inferred from fission track data in the northern Rhenish Massif west of the Rhine (Glasmacher et al. 1998) (Fig. 7b). As these denudation rates integrate over many millions of years, temporal variations in the rate of erosion are smoothed out and cannot be detected by this method. Although the inferred thermal histories have a considerable uncertainty, and their conversion to denudation rates assumes a stable geothermal gradient,

the fission track data yield long-term denudation rates that are similar to our ^{10}Be -based erosion rates, which integrate over the Holocene epoch. This observation suggests that also on a timescale of tens of million of years the landscape remained in or close to a steady state. Cenozoic exhumation and cooling have been interpreted as an isostatic response to former erosion and to a major base-level fall caused by the subsidence of the lower Rhine Basin in the Tertiary (Karg et al. 2005).

In the central part of Rhenish Massif, which belongs to the Eifel region, river terraces along the Rhine indicate that rock uplift has accelerated during the Pliocene and Quaternary and attained a maximum value of ~ 250 mm/ka during the last 800 ka (see Fig. 7b) (Meyer and Stets 1998; van Balen et al. 2000). In this central part of the Rhenish Massif, the presence of narrow, up to 200-m-deep valleys incised into older low-relief surfaces characterizes a landscape that is clearly in disequilibrium, not in a steady state. The strong uplift signal in this region is presumably a combined effect caused by heating of the lithosphere above a mantle plume (e.g., Garcia-Castellanos et al. 2000; Ritter et al. 2001), and the isostatic response to long-term erosion (Karg et al. 2005). Hence, the Rhenish Massif provides an excellent example of a landscape where both equilibrium and disequilibrium landscapes did co-exist over the last several hundred thousand years.

Conclusions

Erosion rates were quantified for two catchments in the northeastern Rhenish Massif, utilizing different analytical approaches: ^{10}Be abundances, river loads, and sediment accumulation in storage basins. Resulting short-term rates, integrating over the past 50 years, are about one-third of the long-term millennial-scale erosion rates. Supplementary modeling clearly indicates that enhanced sediment export during flood events alone cannot explain this discrepancy. Instead, climatic factors such as precipitation/evapotranspiration and related changes in vegetation coverage/soil exposure appear to be of additional importance. The present study further indicates that a full understanding of weathering and erosion, hence, the interaction between atmosphere, hydrosphere and lithosphere, is best achieved via a multidisciplinary approach covering different timescales.

Acknowledgments This research was funded by the German Research Foundation (DFG; grant HE-1704/5-1). We thank the staff of the *Aabach-Talsperre*, the *Ruhrverband*, and the *Umweltamt Lippstadt* for providing the discharge data, and A. Fugmann, L. Hooyman, and B. Romberg for help with the preparation of samples. Constructive reviews by F. Kober and S. Carretier improved the quality of the text and are gratefully acknowledged.

References

- Balco G, Stone JO, Lifton NA, Dunai TJ (2008) A complete and easily accessible means of calculating surface exposure ages or erosion rates from ^{10}Be and ^{26}Al measurements. *Quat Geochronol* 3:174–195. doi:10.1016/j.quageo.2007.12.001
- Beilke S, Uhse K, Jäschke M (2003) Jahresbericht 2002 aus dem Messnetz des Umweltbundesamtes. <http://www.umweltbundesamt.de/publikationen/fpdf-l/2559.pdf>, accessed 16 Jan 2008
- Bierman P, Steig EJ (1996) Estimating rates of denudation using cosmogenic isotope abundances in sediment. *Earth Surf Process Landf* 21:125–139. doi:10.1002/(SICI)1096-9837(199602)21:2<125::AID-ESP511>3.0.CO;2-8
- Bodensystematik AK (1998) Systematik der Böden und bodenbildenden Substrate Deutschlands. *Mitt Dtsch Bodenkd Ges* 86:1–80
- Bork H-R, Bork H, Dalchow C, Faust B, Pierr H-P, Schatz T (1998) Landschaftsentwicklung in Mitteleuropa. Klett-Perthes, Gotha, p 328
- Brown ET, Stallard RF, Larsen MC, Raisbeck GM, Yiou F (1995a) Denudation rates determined from the accumulation of in situ-produced ^{10}Be in the Luquillo Experimental Forest, Puerto Rico. *Earth Planet Sci Lett* 129:193–202. doi:10.1016/0012-821X(94)00249-X
- Brown ET, Bourlès DL, Colin F, Raisbeck GM, Yiou F, Desgarceaux S (1995b) Evidence for muon-induced production of ^{10}Be in near-surface rocks from the Congo. *Geophys Res Lett* 22:703–706. doi:10.1029/95GL00167
- Brown ET, Colin F, Bourlès DL (2003) Quantitative evaluation of soil processes using in situ-produced cosmogenic nuclides. *C R Geosci* 335:1161–1171. doi:10.1016/j.crte.2003.10.004
- Buhl D, Neuser RD, Richter DK, Riedel D, Roberts B, Strauss H et al (1991) Nature and nurture: environmental story of the River Rhine. *Naturwissenschaften* 78:337–346. doi:10.1007/BF01131605
- Busch G, Ewald S (2000) Fläche und tiefe Grundwässer im Warsteiner Massenkalk. In: Protokoll zum Festkolloquium Regionale Beiträge zur Hydrogeologie. insbesondere der Mineral- und Thermalwässer, Roetgen, pp 1–14
- Clausen CD, Leuteritz K (1984) Geologische Karte von Nordrhein-Westfalen, Erläuterungen zu Blatt 4516 Warstein. Geologisches Landesamt Nordrhein-Westfalen, Krefeld, p 155
- Codilean AT (2006) Calculation of the cosmogenic nuclide production topographic shielding scaling factor for large areas using DEMs. *Earth Surf Process Landf* 31:785–794. doi:10.1002/esp.1336
- Cyr AJ, Granger DE (2008) Dynamic equilibrium among erosion, river incision, and coastal uplift in the northern and central Apennines, Italy. *Geology* 36:103–106. doi:10.1130/G24003A.1
- Drever JI (1994) The effect of land plants on weathering rates of silicate minerals. *Geochim Cosmochim Acta* 58:2325–2332. doi:10.1016/0016-7037(94)90013-2
- Dunai TJ (2000) Scaling factors for production rates of in situ produced cosmogenic nuclides: a critical reevaluation. *Earth Planet Sci Lett* 176:157–169. doi:10.1016/S0012-821X(99)00310-6
- EEA (2000) CLC90 100 m, version 12/2000. European Environment Agency (EEA), Copenhagen. <http://www.eea.eu.int>. Accessed 16 January 2008
- Ferrier KL, Kirchner JW, Finkel RC (2005) Erosion rates over millennial and decadal timescales at Caspar Creek and Redwood Creek, Northern California Coast Ranges. *Earth Surf Process Landf* 30:1025–1038. doi:10.1002/esp.1260
- Flintrop C, Hohlmann B, Jasper T, Korte C, Podlaha OG, Scheele S et al (1996) Anatomy of pollution: rivers of North Rhine-Westfalia, Germany. *Am J Sci* 296:58–98
- Franke W (2000) The mid-European segment of the Variscides: tectonostratigraphic units, terrane boundaries and plate tectonic evolution. In: Frank W, Haak V, Oncken O, Tanner D (eds) *Orogenic processes: quantification and modelling in the variscan belt*. Geological Society, London, Special Publications 179:35–61
- Fuchs K, von Gehlen K, Malzer H, Murawski H, Semmel A (1983) Plateau uplift: the Rhenish Shield, a case history. Springer-Verlag, Berlin, p 411
- Garcia-Castellanos D, Cloetingh S, Van Balen R (2000) Modelling the Middle Pleistocene uplift in the Ardennes-Rhenish Massif: thermo-mechanical weakening under the Eifel? *Glob Planet Change* 27:39–52. doi:10.1016/S0921-8181(01)00058-3
- Glasmacher U, Zentilli M, Grist AM (1998) Apatite fission-track thermochronology of Paleozoic sandstones and the Hill-intrusion, northern Linksrheinisches Schiefergebirge, Germany. In: Van den Haute P, De Corte F (eds) *Advances in fission-track geochronology*. Solid earth sciences library vol. 10. Kluwer, Dordrecht, pp 151–172
- Gosse JC, Phillips FM (2001) Terrestrial in situ cosmogenic nuclides: theory and application. *Quat Sci Rev* 20:1475–1560. doi:10.1016/S0277-3791(00)00171-2
- Granger DE, Riebe CS (2007) Cosmogenic nuclides in weathering and erosion. In: Holland HD, Turekian KK (eds) *Surface and ground water, weathering, and soils*. Treatise Geochem 5:1–43
- Granger DE, Kirchner JW, Finkel R (1996) Spatially averaged long-term erosion rates measured from in situ-produced cosmogenic nuclides in alluvial sediment. *J Geol* 104:249–257
- Hack JT (1976) Dynamic equilibrium and landscape evolution. In: Melhorn WN, Flemal RC (eds) *Theories of landform development*. Publications in Geomorphology, Binghamton, pp 87–102
- Heimsath AM (2006) Eroding the land: steady-state and stochastic rates and processes through a cosmogenic lens. In: Siame LL, Bourlès DL, Brown ET (eds) *In situ-produced cosmogenic nuclides and quantification of geological processes*. *Geol Soc Am Special Pap* 415:111–129
- Heisinger B, Lal D, Jull AJT, Kubik PW, Ivy-Ochs S, Neumaier S et al (2002a) Production of selected cosmogenic radionuclides by muons. 1. Fast muons. *Earth Planet Sci Lett* 200:345–355. doi:10.1016/S0012-821X(02)00640-4
- Heisinger B, Lal D, Jull AJT, Kubik PW, Ivy-Ochs S, Knie K et al (2002b) Production of selected cosmogenic radionuclides by muons. 2. Capture of negative muons. *Earth Planet Sci Lett* 200:357–369. doi:10.1016/S0012-821X(02)00640-4
- Hewawasam T, von Blanckenburg F, Schaller M, Kubik P (2003) Increase of human over natural erosion rates in tropical highlands constrained by cosmogenic nuclides. *Geology* 31:597–600. doi:10.1130/0091-7613(2003)031<0597:IOHONE>2.0.CO;2
- Hinderer M (2001) Late Quaternary denudation of the Alps, valley and lake fillings and modern river loads. *Geodin Acta* 14:231–263. doi:10.1016/S0985-3111(01)01070-1
- Hoffmann T, Erkens G, Cohen KM, Houben P, Seidel J, Dikau R (2007) Holocene floodplain sediment storage and hillslope erosion within the Rhine catchment. *Holocene* 17:105–118. doi:10.1177/0959683607073287
- Judson S, Ritter DF (1964) Rates of regional denudation in the United States. *J Geophys Res* 69:3395–3401. doi:10.1029/JZ069i016p03395
- Karg H, Carter A, Brix MR, Littke R (2005) Late- and post-Variscan cooling and exhumation history of the northern Rhenish massif and the southern Ruhr Basin: new constraints from fission-track analysis. *Int J Earth Sci* 94:180–192. doi:10.1007/s00531-005-0467-2
- Kaspar E (1993) Der Feststofftransport der Wutach: Hochwasseranalysen und Frachtbilanzen des Schwebstoff- und Geröllaustrags. *Tübinger Geowissensch Arb* C15:203–215

- Kendall C, Doctor DH (2003) Stable Isotope Applications in Hydrologic Studies. In: Drever JI (ed) Surface and Ground Water, Weathering, and Soils. *Treatise Geochem* 5:319–364
- Kirchner JW, Finkel RC, Riebe CS, Granger DE, Clayton JL, King JG et al (2001) Mountain erosion over 10 yr, 10 k.y., and 10 m.y. time scales. *Geology* 29:591–594. doi:10.1130/0091-7613(2001)029<0591:MEOYKY>2.0.CO;2
- Kober F, Ivy-Ochs S, Schlunegger F, Baur H, Kubik PW, Wieler R (2007) Denudation rates and a topography-driven rainfall threshold in northern Chile: multiple cosmogenic nuclide data and sediment yield budgets. *Geomorphology* 83:97–120. doi:10.1016/j.geomorph.2006.06.029
- Koch M, Michel G, Schröter H (1974) Zur Hydrogeologie des Warsteiner Massenkalk-Gebietes (Nordöstliches Sauerland). *Fortschr Geol Rheinl Westfal* 20:195–214
- Kohl CP, Nishiizumi K (1992) Chemical isolation of quartz for measurement of in situ-produced cosmogenic nuclides. *Geochim Cosmochim Acta* 56:3583–3587. doi:10.1016/0016-7037(92)90401-4
- Kubik PW, Ivy-Ochs S, Masarik J, Frank M, Schlüchter C (1998) ^{10}Be and ^{26}Al production rates from an instantaneous event within the dendro-calibration curve, the landslide of Köfels, Ötztal Valley, Austria. *Earth Planet Sci Lett* 161:231–241. doi:10.1016/S0012-821X(98)00153-8
- Lal D (1991) Cosmic ray labelling of erosion surfaces: in situ nuclide production rates and erosion models. *Earth Planet Sci Lett* 104:424–439. doi:10.1016/0012-821X(91)90220-C
- Laslett GM, Galbraith RF (1996) Statistical modelling of thermal annealing of fission-tracks in apatite. *Geochim Cosmochim Acta* 60:5117–5131. doi:10.1016/S0016-7037(96)00307-9
- Lenzi MA, Marchi L (2000) Suspended sediment load during floods in a small stream of the Dolomites (northeastern Italy). *Catena* 39:267–282. doi:10.1016/S0341-8162(00)00079-5
- Macaire J-J, Bossuet G, Choquier A, Cocirca C, de Luca P, Dupis A et al (1997) Sediment yield during Late Glacial and Holocene periods in the Lac Chambon watershed, Massif Central, France. *Earth Surf Process Landf* 22:472–489. doi:10.1002/(SICI)1096-9837(199705)22:5<473::AID-ESP710>3.0.CO;2-I
- Martin Y (2003) Evaluation of bed load transport formulae using field evidence from the Vedder River, British Columbia. *Geomorphology* 53:75–95. doi:10.1016/S0169-555X(02)00348-3
- Matsuoka N (1998) Modelling frost creep rates in an Alpine environment. *Permafrost Periglacial Process* 9:397–409. doi:10.1002/(SICI)1099-1530(199810/12)9:4<397::AID-PPP302>3.0.CO;2-Q
- Meiburg P (1979) Terrassen-Niveaus und Vertikalbewegungen im Diemel-Gebiet. In: Protokoll zum 3. Kolloquium im DFG Schwerpunkt Vertikalbewegungen und ihre Ursachen am Beispiel des Rheinischen Schildes, Neustadt, 20–25
- Meyer W, Stets J (1998) Junge Tektonik im Rheinischen Schiefergebirge und ihre Quantifizierung. *Z Dtsch Geol Ges* 149:359–379
- Milde B (1996) Auswirkungen auf den Naturhaushalt. In: Westphal W, Prien KJ, Milde B, Bartmann L (eds) Die Aabach-Talsperre: Auswirkungen auf Landschaft, Wasserwirtschaft, Naturhaushalt und Fischerei. Schriftenreihe des Westfälischen Amtes für Landes- und Baupflege 11:33–53
- Milliman JD, Syvitski JPM (1992) Geomorphic/tectonic control of sediment discharge to the ocean: the importance of small mountainous rivers. *J Geol* 100:525–544
- Morel P, von Blanckenburg F, Schaller M, Kubik PW, Hinderer M (2003) Lithology, landscape dissection and glaciation controls on catchment erosion as determined by cosmogenic nuclides in river sediment (the Wutach Gorge, Black Forest). *Terra Nova* 15:398–404. doi:10.1046/j.1365-3121.2003.00519.x
- Négrel P, Allègre CJ, Dupré B, Lewin E (1993) Erosion sources determined by inversion of major and trace element ratios in river water: the Congo Basin case. *Earth Planet Sci Lett* 120:59–76. doi:10.1016/0012-821X(93)90023-3
- Pimentel D, Harvey C, Resosudarmo P, Sinclair K, Kurz D, McNair M et al (1995) Environmental and economic costs of soil erosion and conservation benefits. *Science* 267:1117–1123. doi:10.1126/science.267.5201.1117
- Rickenmann D (1997) Sediment transport in swiss torrents. *Earth Surf Process Landf* 22:937–951. doi:10.1002/(SICI)1096-9837(199710)22:10<937::AID-ESP786>3.0.CO;2-R
- Riebe CS, Kirchner JW, Granger DE, Finkel RC (2001) Strong tectonic and weak climatic control of long-term chemical weathering rates. *Geology* 29:511–514. doi:10.1130/0091-7613(2001)029<0511:STAWCC>2.0.CO;2
- Riebe CS, Kirchner JW, Finkel RC (2004) Erosional and climatic effects on long-term chemical weathering rates in granitic landscapes spanning diverse climate regimes. *Earth Planet Sci Lett* 224:547–562. doi:10.1016/j.epsl.2004.05.019
- Ritter JRR, Jordan M, Christensen UR, Achauer U (2001) A mantle plume below the Eifel volcanic fields, Germany. *Earth Planet Sci Lett* 186:7–14. doi:10.1016/S0012-821X(01)00226-6
- Rovira A, Batalla RJ (2006) Temporal distribution of suspended sediment transport in a Mediterranean basin: the lower Tordera (NE SPAIN). *Geomorphology* 79:58–71. doi:10.1016/j.geomorph.2005.09.016
- Roy S, Gaillardet J, Allègre CJ (1999) Geochemistry of dissolved and suspended loads of the Seine river, France: anthropogenic impact, carbonate and silicate weathering. *Geochim Cosmochim Acta* 63:1277–1292. doi:10.1016/S0016-7037(99)00099-X
- Schaller M, von Blanckenburg F, Hovius N, Kubik PW (2001) Large-scale erosion rates from in situ-produced cosmogenic nuclides in European river sediments. *Earth Planet Sci Lett* 188:441–458. doi:10.1016/S0012-821X(01)00320-X
- Schaller M, von Blanckenburg F, Veldkamp A, Tebbens LA, Hovius N, Kubik PW (2002) A 30,000 yr record of erosion rates from cosmogenic ^{10}Be in Middle European river terraces. *Earth Planet Sci Lett* 204:307–320. doi:10.1016/S0012-821X(02)00951-2
- Schmidt KH, Morche D (2006) Sediment output and effective discharge in two small high mountain catchments in the Bavarian Alps, Germany. *Geomorphology* 80:131–145. doi:10.1016/j.geomorph.2005.09.013
- Semmel A (1968) Studien über den Verlauf jungpleistozäner Formung in Hessen. *Frankf Geogr Hefte* 45:1–133
- Summerfield MA, Hulton NJ (1994) Natural controls of fluvial denudation rates in major world drainage basins. *J Geophys Res* 99:13871–13883. doi:10.1029/94JB00715
- Synal HA, Bonani G, Dobeli M, Ender RM, Gartenmann P, Kubik PW et al (1997) Status report of the PSI/ETH AMS facility. *Nucl Instrum Methods Phys Res B* 123:62–68. doi:10.1016/S0168-583X(96)00608-8
- Vanacker V, von Blanckenburg F, Govers G, Molina A, Poesen J, Deckers J et al (2007) Restoring dense vegetation can slow mountain erosion to near natural benchmark levels. *Geology* 35:303–306. doi:10.1130/G23109A.1
- Van Balen RT, Houtgast RF, Van der Wateren FM, Vandenberghe J, Bogaart PW (2000) Sediment budget and tectonic evolution of the Meuse catchment in the Ardennes and the Roer Valley Rift System. *Glob Planet Change* 27:113–129. doi:10.1016/S0921-8181(01)00062-5
- Völkel J (1995) Periglaziale Deckschichten und Böden im Bayrischen Wald und seinen Randgebieten als geogene Grundlagen landschaftsökologischer Forschung im Bereich naturnaher Waldstandorte. *Z Geomorph N F* 96(Suppl):1–301
- Von Blanckenburg F (2006) The control of erosion and weathering at basin scale from cosmogenic nuclides in river sediment. *Earth Planet Sci Lett* 242:223–239. doi:10.1016/j.epsl.2005.10.007

- Wigley TM, Plummer LN, Pearson FJ (1978) Mass transfer and carbon isotope evolution in natural water systems. *Geochim Cosmochim Acta* 42:1117–1139. doi:[10.1016/0016-7037\(78\)90108-4](https://doi.org/10.1016/0016-7037(78)90108-4)
- Willet SD, Brandon MT (2002) On steady states in mountain belts. *Geology* 30:175–178. doi:[10.1130/0091-7613\(2002\)030<0175:OSSIMB>2.0.CO;2](https://doi.org/10.1130/0091-7613(2002)030<0175:OSSIMB>2.0.CO;2)
- Wittmann H, von Blanckenburg F, Kruesmann T, Norton KP, Kubik PW (2007) Relation between rock uplift and denudation from cosmogenic nuclides in river sediment in the Central Alps of Switzerland. *J Geophys Res* 112:F04010. doi:[10.1029/2006JF000729](https://doi.org/10.1029/2006JF000729)
- Wortmann H (1937) Die Terrassen der Diemel zwischen Sauerland und Weser. *Jahrb preuss geol Landesanst* 57:359–413
- Zolitschka B (1998) A 14, 000-year sediment yield record from western Germany based on annually laminated lake sediments. *Geomorphology* 22:1–17. doi:[10.1016/S0169-555X\(97\)00051-2](https://doi.org/10.1016/S0169-555X(97)00051-2)
- Zolitschka B (2002) Late Quaternary sediment yield variations—natural versus human forcing. *Z Geomorph N F* 128(Suppl):1–15